

Research Article

Impacts of Climate Change on Temperature and Rainfall on Dawa Sub-watershed, Genale Dawa River Basin, Southern Ethiopia

Ayana Bulti^{1, 2, *} , Fentaw Abegaz³

¹Oromia Agricultural Research Institute, Mechara Agricultural Research Center, Department of Irrigation and Drainage Engineering, Mechara, Ethiopia

²School of Water Resource and Environmental Engineering, Haramaya University Institute of Technology, Dire Dawa, Ethiopia

³Independent Researcher, Adama, Ethiopia

Abstract

Understanding how climate change affects the frequency and length of temperature and rainfall is global issue. Climate change is statistical variations over an extended period in the features of the climate system, such as variations in global temperatures and precipitation, caused by human and natural sources. In this work coordinated regional climate downscaling experiment for Africa, which integrates climate forecasts from Coupled Model Intercomparison Project5 based on an ensemble of GCM-RCM model was used to statistically downscale the climate change scenarios. This study aimed to estimate climate change impacts on temperature and rainfall. The impact of climate change has been evaluated by reporting under RCP4.5 and 8.5 scenarios. For the extraction and bias correction of the daily maximum and minimum temperature, as well as rainfall of 30-year overlap periods, CMhyd has been employed. The annual minimum temperatures are predicted to increase by 2.94, 3.45, 3.21, and 3.59 °C and annual maximum temperatures increased by 2.61, 2.83, 2.71 and 3.36 °C for RCP4.5 and RCP8.5 respectively. The change in rainfall reveals annual average decreases of 8.45 to 9.3% and 10.5 to 10.95% at RCP4.5 and 8.5, respectively. Considering the evaluated parameters, minimum and maximum temperatures increased trends but for the rainfall, large fluctuations were predicted. Moreover, in the study years for the parameters in all simulated models, the RCP8.5 scenario estimated a higher amount than the RCP4.5 scenario. Implement various trees, apply water harvesting structure, Surface runoff harvesting and more multiple GCM-RCM driving models with various RCM outputs to improve more prediction accuracy in the future studies.

Keywords

Climate Change, CMhyd, CORDEX AFRICA, Genale Dawa Watershed, Ethiopia

*Corresponding author: ayanabub@gmail.com (Ayana Bulti)

Received: 26 July 2024; **Accepted:** 24 August 2024; **Published:** 20 September 2024



Copyright: © The Author(s), 2024. Published by Science Publishing Group. This is an **Open Access** article, distributed under the terms of the Creative Commons Attribution 4.0 License (<http://creativecommons.org/licenses/by/4.0/>), which permits unrestricted use, distribution and reproduction in any medium, provided the original work is properly cited.

1. Introduction

Climate change is the statistical variations over an extended period in the features of the Climate system caused by natural or human factors, such as variations in global temperatures, precipitation, etc. Climate change has the potential significantly disrupt the quantity and quality of natural resources, which would harm people's ability to secure a living [22]. The rise in temperature due to global climate change has far-reaching effects on both humans and ecosystems [32]. With a rising temperature and evaporative requirement, the warming trend and climate variability have an impact on agricultural output. More than 95% of the output of rain-fed crops grown by tenacious smallholder farmers are impacted by climate change and have little ability to adjust [4].

The global mean surface temperature has been rising since the late nineteenth century, according to historical temperature data, with the last three decades being consistently higher than any of the preceding decades [13]. General circulation models (GCMs) are extensively employed for studying climate change on global and regional scales [36, 34]. These models generate climate scenarios for both current and future time periods. Additionally, GCMs are valuable for assessing the hydrological impacts resulting from changes in climate variables [21, 27-29]. The analysis of GCM outputs indicates that regions currently experiencing dry conditions are likely to become even drier, while wetter areas may become wetter. Additionally, there is a noticeable expansion of arid and semi-arid climates [10, 31]. Nevertheless, a comprehensive investigation of regional and seasonal impacts of CC in the

future is needed, particularly at regional scales [3]. Although previous studies provide essential information about potential CC impacts [15, 18, 24, 35] our understanding of CC impact on the hydrological characteristic.

Climate change is currently one of the world's most pressing issues [5, 37, 38]. This is especially true for Sub-Saharan Africa, which has a limited capacity to counteract its impacts. Given that, the majority of Africa's population lives in rural regions and relies mostly on rain-fed agriculture for a living, climate variability and changes, as well as accompanying droughts and floods, have a direct impact on agricultural production and food security. As a result, climate change poses a threat to all elements of human development, including the natural environment and social vulnerability [26].

2. Materials and Methods

2.1. Description of the Study Area

The location of the Dawa River watershed is $38^{\circ} 2' 48''$ to $41^{\circ} 2' 34''$ E and $4^{\circ} 5' 8''$ to $6^{\circ} 27' 18''$ N (Figure 1) It makes up a portion of Ethiopia's southeast highlands and is located 567 kilometers southwest of Addis Ababa. The Dawa River Sub-watershed is located in East Africa and flows through Kenya, Ethiopia, and Somalia, with 81% falling into Ethiopian territory.

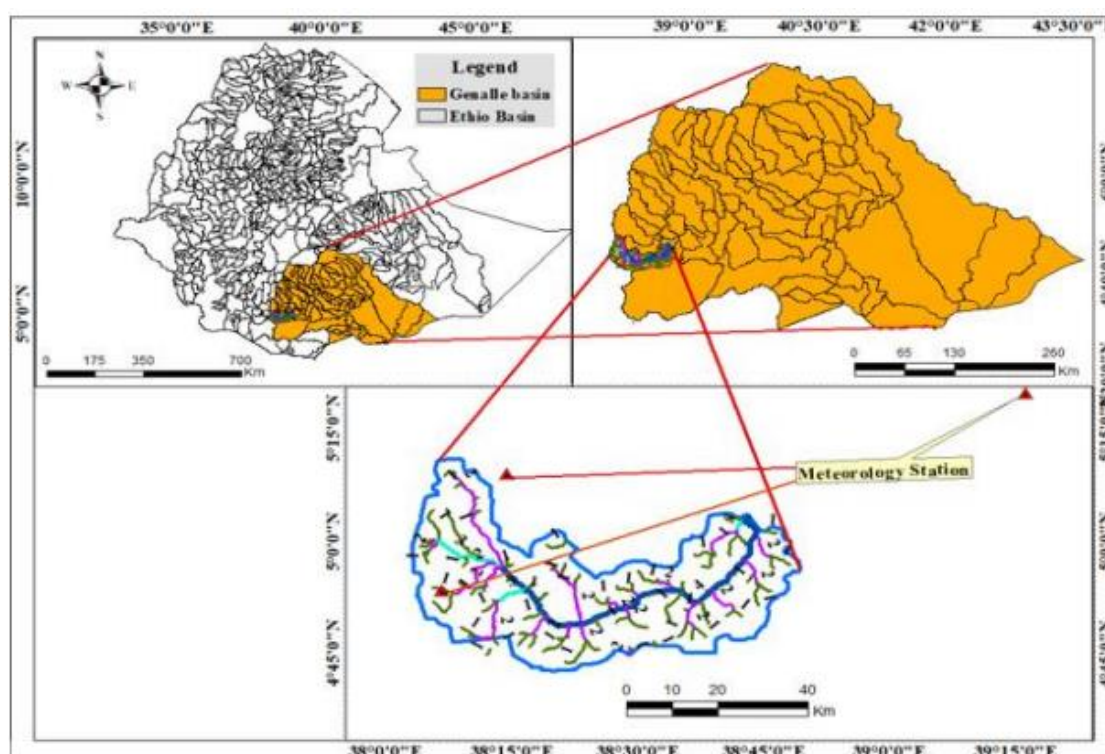


Figure 1. Location Map of the Study area (Source: Ethiopian Geospatial Map, 2016).

Table 1. Summary of the meteorological stations.

Station name	Data Length	Elevation (m)	Latitude (°)	Longitude (°)	Rainfall (mm)	Temp. (°C)	Missed (%)	Remark
Yabello	1990-2020	1729	4.89	38.10	651	19.8	8.47	Filled
Hageremariam	1990-2020	1729	5.15	38.23	947	19.5	5.55	Filled
Kibre Mengist	1990-2020	1861	5.86	38.96	1673	19.4	7.56	Filled
Negalle	1990-2020	1439	5.33	39.26	710	20.9	6.54	Filled
Oda Shakiso	1990-2020	1620	5.83	38.96	1020	18.5	9.45	Filled
Mega	1990-2020	1607	4.03	38.33	720	19.5	7.54	Filled

2.2. Generation of Climate Data

To investigate the catchment-drainage networks, the DEM was used to provide a variety of data that helped produce a map of the landforms, soil types, and hydrologic information. The topography of the study areas is typically represented by a 12.5m by 12.5m Digital Elevation Model (DEM) acquired from the SRTM.

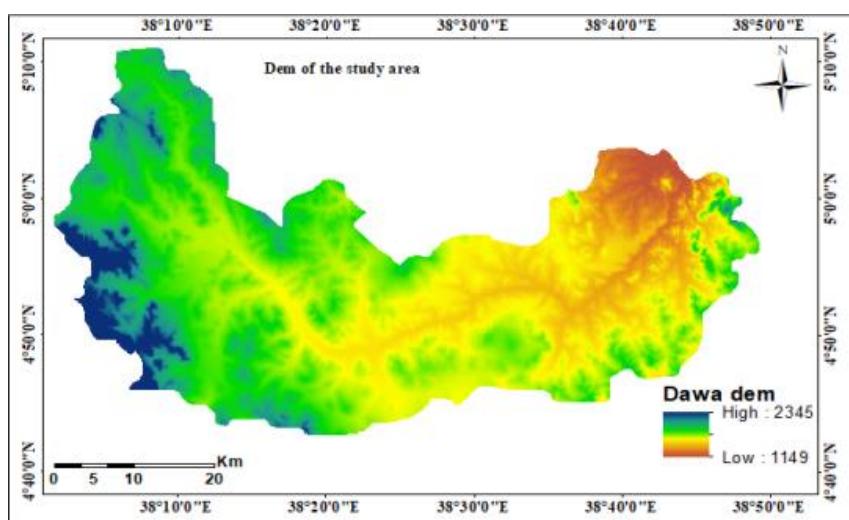
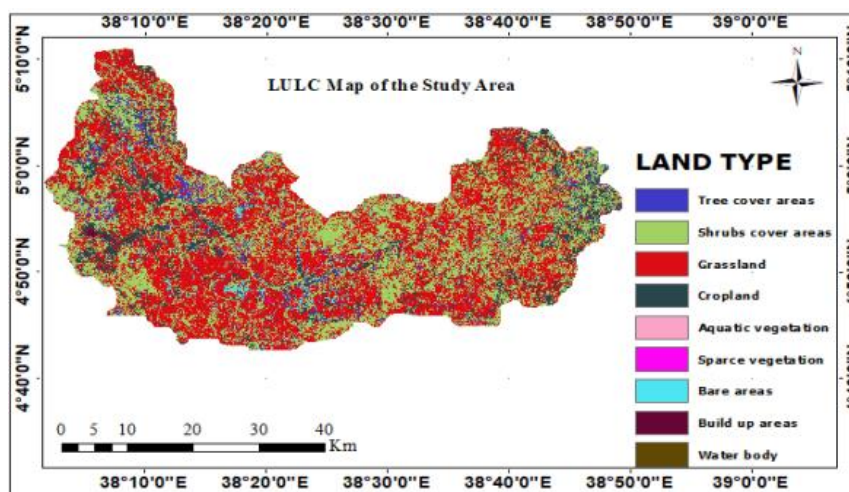
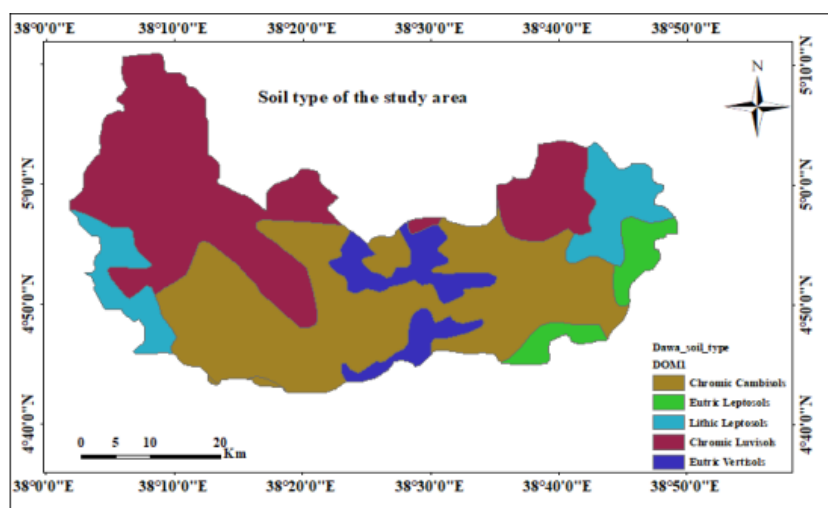
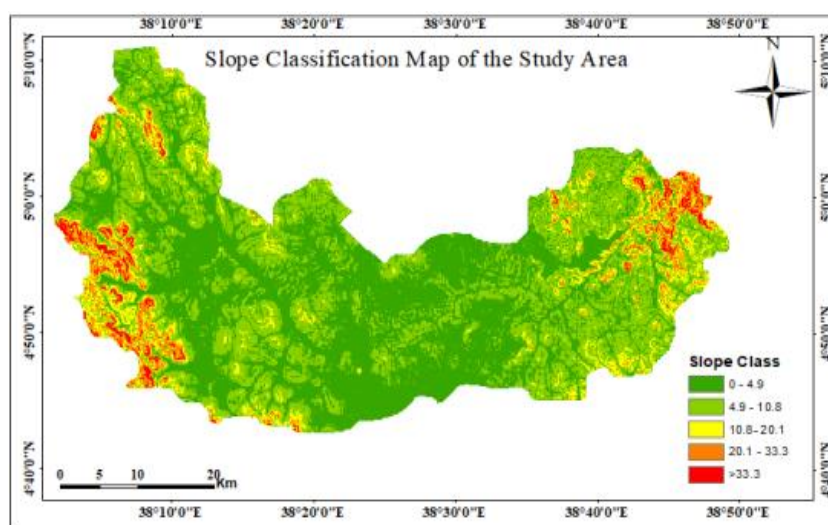
**Figure 2.** DEM of study area.**Figure 3.** LULC map.

Table 2. LULC and soil classification and area covered by watershed.

LULC			Soil			
LULC type	Area (ha)	Area (%)	Soil type	Code	Area (ha)	Area (%)
Tree cover	10112	4.3	Chromic Cambisols	CMx	98032	41.5
Shrubs cover	86543	36.7	Chromic Luvisols	LXx	85854	36.3
Grassland	110428	46.9	Lithic Leptosols	LPq	24630	10.4
Cropland	24863	10.6	Eutric Vertisols	VRe	17408	7.4
Flooded	4.54	0.002	Eutric Leptosols	LPe	10506	4.4
Sparse vegetation	62.95	0.03				
Bare areas	3518	1.5				
Build up areas	204	0.1				
Waterbody	30	0.01				

**Figure 4.** Soil-type map.**Figure 5.** Slope classification study area.

Slope and Elevation Zone

The slope has demonstrated this in many ranges in the study region. It covers a wide range of values throughout the entire research watershed. The elevation zone has demonstrated this in many ranges in the study region. It covers a wide range of values in the entire watershed.

Table 3. Division of watershed into different elevation zones.

Zone	Elevation ranges (m)		Elevation
	Min	Max	
1	1149	1393	574.5
2	1393	1523	761.5
3	1523	1638	1535.5
4	1638	1834	1736
5	1834	2345	2089.5

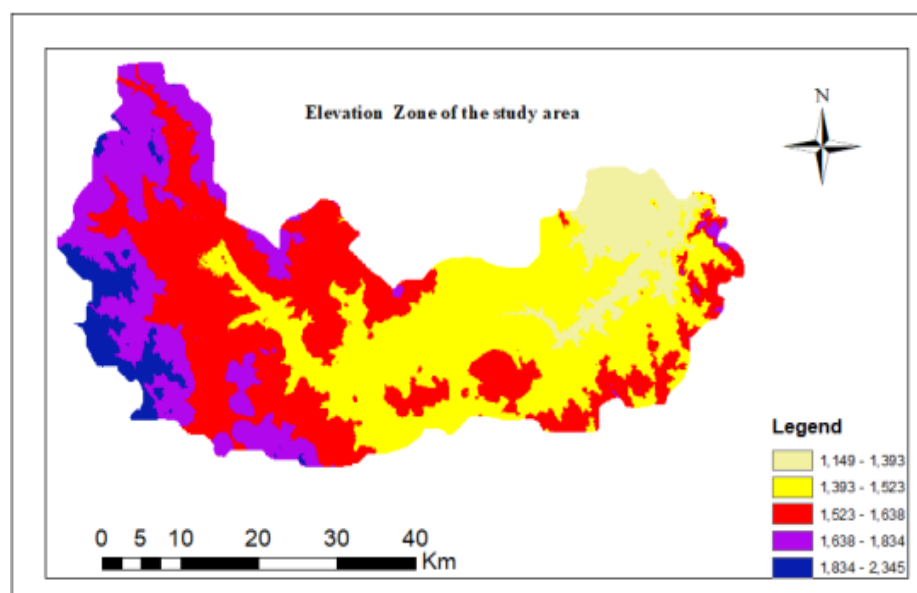


Figure 6. Elevation of study area.

2.3. Methods and Analysis of Data Collection

The base period of required meteorological data of daily precipitation and maximum and minimum temperature was collected from the NMA office and downloaded from the CORDEX East Africa database using an ensemble of RCM model output. Observation data for the modelling of the work, such as monthly meteorological data over 30 years from 1976 to 2020 obtained from NMSA. Historical precipitation and temperature data for the same period (1976-2005) were retrieved from an ensemble of RCM-GCMs. The RCM-GCM simulations run in the framework of the Coordinated Regional Climate Downscaling Experiment (CORDEX Africa,

<https://cordex.org/>. Future temperature and precipitation projections for the period 2020 (2025-2054) and 2050 (2055-2084) were retrieved from the same RCM GCM combinations. The Representative Concentration Pathways RCP 4.5 and RCP 8.5 [23] were used for future scenarios for the study areas. Most of the models were limited to the simulation of local precipitation, although other variables, such as temperature, humidity, and wind are usually required for hydrological simulations. Long-term precipitation patterns in Ethiopia are difficult to determine due to high unpredictability; nonetheless, an overall drop was recorded in the last three to four decades, with significant year-to-year fluctuation.

2.4. Models and Software Used

ArcGIS 10.4 version used for extracting study area, LULC, soil type, elevation and Ensembles of RCM model output for impact assessment, CMhyd software for both extraction and bias correction of CORDEX climate data, and XLSTAT for homogeneity test used to achieve the study's goal. In addition to the model two scenarios, RCP4.5 and RCP 8.5 used. This is due to RCP4.5 as a medium stabilization scenario and RCP8.5 as a pessimistic and the latest climate scenario. The maximum and minimum temperatures were interpolated using liner interpolation and the arithmetic mean method for precipitation data. As a result, future climate change scenarios, an ensemble of RCM model output retrieved via two emission scenarios RCP4.5 and RCP8.5 from Cordex Africa. As cited by Gebrie Geremew and Engida Agizew (2015) the grounds for choosing these two scenarios are that RCP4.5 presents an intermediate emission scenario and RCP8.5 shows a high emission scenario of GHG concentrations, and most previous research has been done using these scenarios, for example [12]. Thus, in this work, the ensemble of RCM model output is used to generate future scenarios utilizing RCP4.5 and RCP8.5 scenarios.

2.5. Goodness of Fit Tests

The goodness of fit test is a statistical technique used to determine whether sample data fits a distribution from a certain population. It evaluates how well-observed data align with the expected values from a statistical model. A high goodness of fit indicates that the observed values are close to the model's expected values; while a low goodness of fit shows that, the observed values are relatively far from the expected values. A goodness of fit measure summarizes the size of the differences between the observed data and the model's expected values, and a goodness of fit test determines whether the differences are statistically significant [14].

2.6. Root Mean Square Error

The optimal bias Correction techniques were determined using statistical GOF tests. Here is a list of the terms used to describe RMSE and PBIAS GOF tests: Y_t and F_t represent observed and simulated climatology at time unit t , Y and F represent the mean of observed and simulated climatology over the entire period, and n represents the total number of years in the dataset. It is the most commonly used error statistics test. The RMSE value closer to zero indicates better performance of the model. The RMSE value is given by the following equation:

$$RMSE = \sqrt{\frac{\sum_{t=1}^T (Y_t - F_t)^2}{n}} \quad (1)$$

Where n is the total number of years in the dataset, and Y_t and F_t stand for observed and simulated climatology at time unit t .

2.7. Percent of Bias and Bias Correction Methods

It provides a hint as to the error's general propensity in the simulated data. The accuracy of the model simulation increases with the magnitude of PBIAS's distance from zero. Positive.

PBIAS values imply an underestimation of model bias, whereas negative values denote an overestimation of bias. The PBIAS result is presented as a percentage and as follows:

$$PBIAS = \left[\frac{\sum_{t=1}^T (Y_t - F_t)}{\sum_{t=1}^T Y_t} \right] * 100 \quad (2)$$

The formulas used for rainfall and temperature bias correction are indicated in the Equations below respectively

$$P_{bc} = P_p + \frac{P_o}{P_r} \quad (3)$$

$$T_{bc} = T_p + T_o - T_r \quad (4)$$

Where P_{bc} is bias-corrected future rainfall amount in mm, P_p is predicted future rainfall amount in mm, P_o is the mean of observed rainfall amount in mm, and P_r is the mean of computed downloaded rainfall during the observation period in mm. T_{bc} is the bias-corrected future temperature in °C; T_p is the predicted future temperature (°C); T_o is the mean of observed temperature in °C; T_r is the mean of computed downloaded temperature during the observed period in °C. Furthermore, correction factors for both precipitation and temperature were computed for each month using the Mean Absolute Error (MAE) method. A positive difference means that the downloaded value is wetter /warmer than the observed precipitation/temperature values for that specific locality. The average monthly precipitation and temperature difference between the observations and the simulation given by the equation:

$$MAE = \frac{1}{N} \sum_{i=1}^N P_{simu} - P_{obse} \quad (5)$$

$$MAE = \frac{1}{N} \sum_{i=1}^N T_{simu} - T_{obse} \quad (6)$$

where, MAE = Mean Absolute Error; N = the number of months; $P_{simu, i}$ = the precipitation for projection at month i and; $P_{obs, i}$ = the precipitation for the observations at month i ; $T_{simu, i}$ = temperature for projection at month i and; $T_{obs, i}$ = temperature for the observations at month i .

2.8. Coefficient of Variation

To assess the inter-annual variability of seasonal and annual rainfall, the CV was used to determine the rainfall variability for the meteorological station:

$$CV = \frac{\delta}{\bar{x}} \quad (7) \quad \text{rainfall as used by [8].}$$

Where, CV= coefficient of variations, δ = standard deviation, and \bar{x} = mean. When $CV < 20\%$ indicates low rainfall variability, CV between 20%to 30% indicates moderate rainfall variability, $CV > 30\%$ indicates high rainfall variability, $CV > 40\%$ very high rainfall variability, and $CV > 70\%$ indicates extremely high rainfall inter-annual variability of

3. Results and Discussions

3.1. Data Quality Control and Adjustments for Further Investigations

Homogeneity Test

Table 4. Summary Statistics of Standard Normal Homogeneity Test.

Station	Variable	Observation	Mean	Standard deviation	Statistics derives	Alpha	P-value
Yabello	Rainfall	45	644.3	133.5	4.90	0.05	0.219

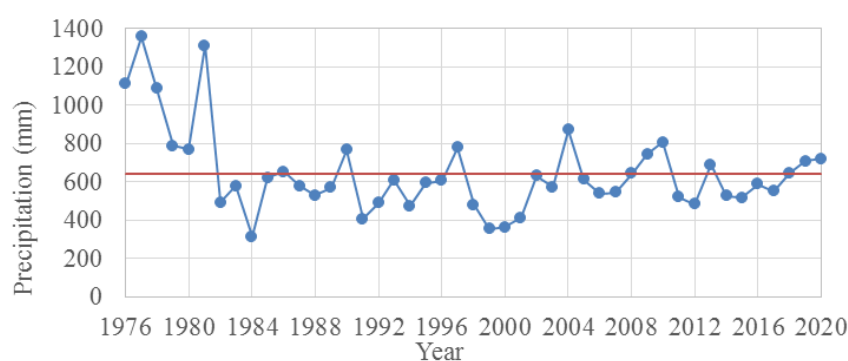


Figure 7. Homogeneity test for Yabello rainfall stations.

Before the climatic data used for further use and research, the missing data filled in utilizing a variety of ways before employing meteorological stations for additional research, it is essential to evaluate the homogeneity. Using the XLSTAT 2022 program, the Standard Normal Homogeneity test (SNHT) was used to

evaluate the homogeneity of annual rainfall data for a station. According to the table below, the bigger p-value from significance level alpha and the red horizontal broken line in the figure reflect rainfall station homogeneity.

Consistency Test

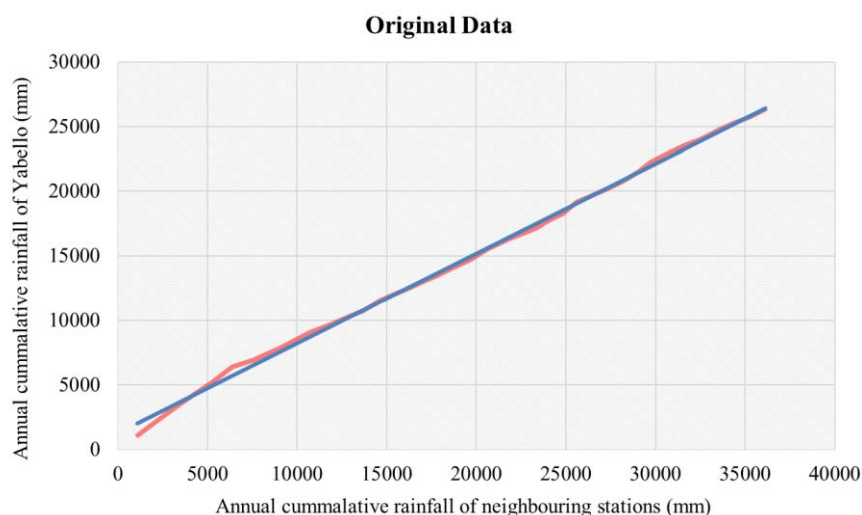


Figure 8. Graph of consistency test of the stations before correction.

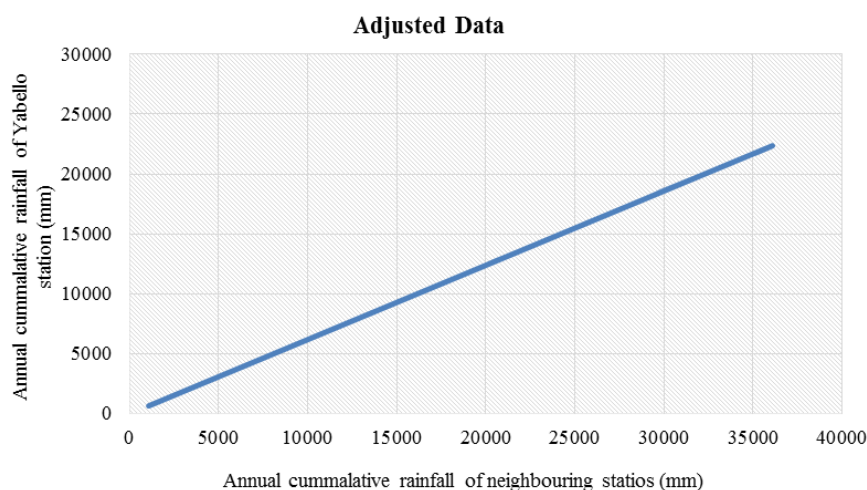


Figure 9. Graph of consistency test of the stations after correction.

The consistency of selected rainfall stations was used as a two-fold/double mass curve analysis approach to check. To test the consistency of the meteorological data with neighboring meteorological stations and to see the uniformity, it was checked with double mass curve analysis (Subramanian, 1998). The accumulated totals of the gauge in question are compared with the corresponding totals for a group of nearby gauge stations. If a significant change in the regime of the curve is observed, it has to be corrected. For this study, the collected data was inconsistent as depicted in Figure 8 and adjusted as shown in Figure 9 before further investigations.

Criteria for Bias Correction Methods

The results of the determination of the percent of biases and RMSE for precipitation and temperature are shown in Tables 5. The difference between the observed and the adjusted control data was calculated by RMSE. According to the data, Delta change strategy appears to have no mistake with observed data, although the Power transformation of precipitation and Linear scaling approaches have considerably lower deviations of 0.032 and 0.078, respectively. Contrarily, the Distribution mapping method has a low variance, whereas the Precipitation local intensity scaling approach has a relatively high deviation of 98.94. Therefore, it may concluded that the Power transformation of the precipitation bias correction method outperforms others. This result is agreed with the findings of [14]. In light of the aforementioned findings, the Delta change technique should not employed

for this work because it equalized the observation data with the present state. It has been shown in almost all of the investigations that the linear scaling and PT techniques have good agreement with the observed data. Although mean biases are taken into account by linear scaling, variance biases are not addressed. It is therefore possible to conclude that the Power transformation of the precipitation technique can used to change the study's future estimations for rainfall. This work is supported by [14]. The amount of rainfall decreased by 0.066 mm using the linear scaling approach and by 0.082 mm using the power transformation of precipitation, which demonstrates negative bias. The amount of rainfall had decreased by 85.83 mm by the Precipitation local intensity scaling approach, which likewise has a large negative bias. The amount of rainfall was increased by 36.31 mm by the Distribution mapping approach, which produces a high positive bias. According to the bias calculation, the Power transformation of the precipitation approach and the Linear scaling method are thought to be the best agreements for temperature fit and bias correction, respectively. The same procedure for the temperature linear scale was selected with an RMSE of 0.051 and PBIAS was 0.035. This result agreed with the findings of [14] are used to describe RMSE and PBIAS. The Power Transformation of the Precipitation Method for Precipitation and Linear Scaling Methods for Temperature selected based on GOF test criteria as Table 5.

Table 5. RMSE and PBIAS for bias correction methods for Precipitation.

Bias correction Methods	Precipitation		Temperature	
	RMSE	PBIAS	RMSE	PBIAS
Linear scaling (multiplicative)	0.078	-0.066	0.051	-0.035
Precipitation local intensity scaling	98.94	-85.83	75.85	-64.5

Bias correction Methods	Precipitation		Temperature	
	RMSE	PBIAS	RMSE	PBIAS
Power transformation of precipitation	0.032	-0.082	35.8	45.6
Distribution mapping of prec. and temp.	28.92	36.31	0.091	-0.065
Delta change correction	0.0	0.0	0.0	0.0

3.2. Regional Climate Model Improvements with Bias Correction

When compared to the average mean monthly rainfall and temperatures (Figure 10 on the left panel), the outputs of the raw regional climate models underestimate and overestimate the mean monthly rainfall and temperatures, respectively.

The Power Transformation of Precipitation Method for Precipitation and Linear Scaling Methods for Temperature in Figures 11 and 12 on the right exhibit good agreement and provide suitable correction for these outputs respectively. This suggests that the model's bias-corrected output accurately depicts the research area's representativeness. This work complies with an agreement with [5].

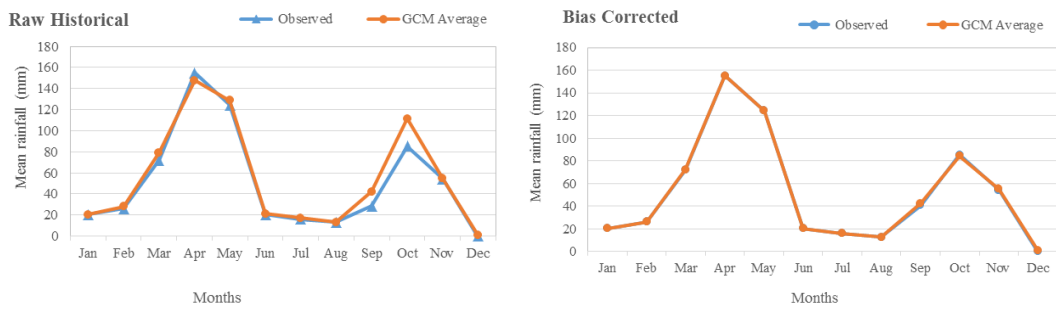


Figure 10. A comparison of the simulated and observed mean monthly rainfall before and after bias adjustment can be seen on the left and right.

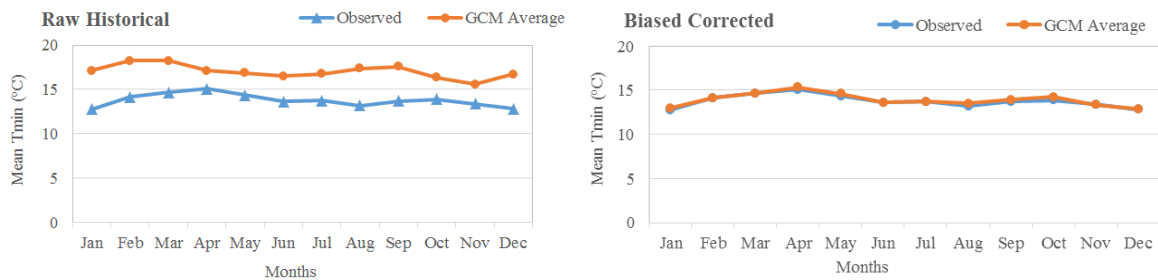


Figure 11. Comparison of bias-corrected mean monthly T_{min} before (left side) and after (right side) simulation and observation.

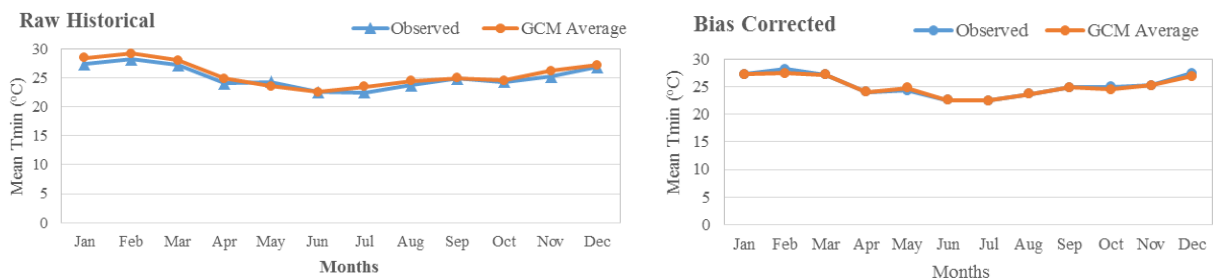


Figure 12. Comparison of bias-corrected simulated and observed mean monthly T_{max} before (left side) and after (right side).

3.3. Predicted Future Rainfall with Comparison to the Baseline Period

Rainfall was calculated using bias-corrected future climate data for the base period and the 2020 and 2050 climate scenarios (Figure 13). The outcome demonstrates that rainfall ranges between 0 to 155, 7.58 to 131.1, and 8.3 to 149.8 mm per month for the base period, RCP4.5 (2020) and 2050, with the lowest and highest values recorded in December and April, respectively. Similarly, for the same above base period, RCP8.5 (2020) and 2050, respectively, range from 3.9 to 146.5, and 9.2 to 140.8 mm/month.

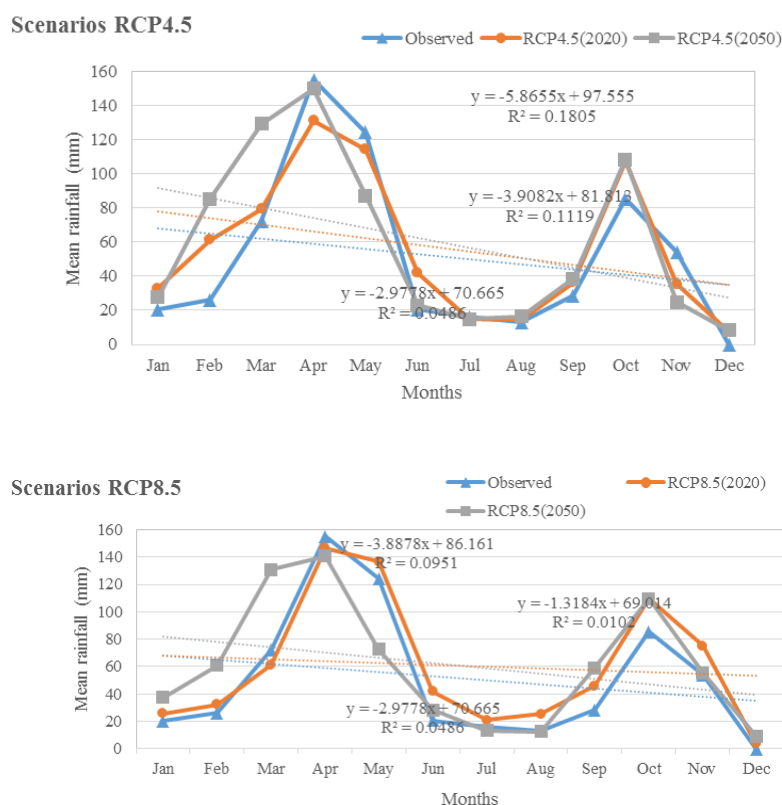


Figure 13. Rainfall at base period, 2020 and 2050 scenarios periods in the study area.

3.4. Variability and Trends of Monthly, Seasonal and Annual Observed Rainfall

Rainfall varies greatly on a yearly and monthly basis, with six months mean January, February, June, July, August, and December out of the twelve months receiving less than 20 mm per month on average from 1991-2020. On the other side, April, followed by October, is the month with the highest mean rainfall (147.2 mm), during the same period (119.6 mm). This works concedes with work of [30]. Rainfall in Yabello is highly variable, as indicated by the computed CV value of 34.45%, while the coefficient of variation for all months spans between 49.4 to 387.5%. Particularly, the CV values that exceed 100% for the research area's months of January, February, March, June, July, August, and December

show that rainfall has an exceptionally high inter-annual variability due to $CV > 70\%$. These findings are consistent results with those reported by [8]. During March, October, and November, the rainfall trend significantly increased ($P\text{-value} > 0.05$) (Figure 14). The slope estimations for March, October, and November showed 0.46, 0.3, and 0.46 respectively. These months show the largest changes in magnitude. For the remaining months over the research years, there is no monotonic trend ($P_{\text{value}} > 0.05$) except for January, February August and October. This discovery is consistent with those that have been reported by [19]. The seasonal distribution of rainfall reveals that *Birra/Belg* (February to May), which recorded a mean precipitation of 355.9 mm, is followed by *Bona* (October to January), which experienced a mean record of 198.4 mm. However, *Ganna* (June to September) was the period for the lowest with 89.9mm.

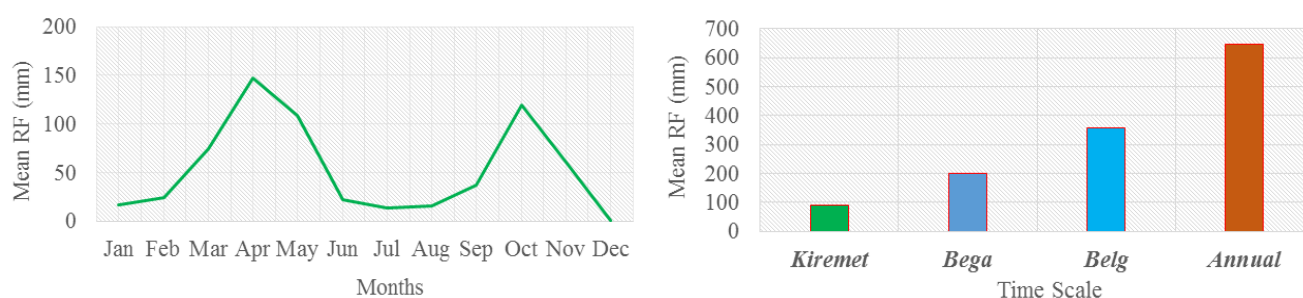


Figure 14. Mean monthly, seasonal and annual observed RF in Yabello.

3.5. Variability and Trends of Predicted Monthly, Seasonal and Annual Rainfall

Rainfall varies monthly, with July, August, and December receiving less than 20 mm per month on average for both RCP (4.5) 2020 and 2050. On the other side, April is the month with the highest mean rainfall 131.1 and 149.8 mm respectively for both scenarios. Rainfall is highly variable, as

indicated by the computed CV value of 31.4% on an annual basis, while the coefficient of variation for all months spans between 49.7 to 183.4% for RCP4.5 (2020) and the computed CV value of 27% is moderate rainfall variability and coefficient of variation for all month's spans 54.8 to 214.2 for RCP4.5 (2050). Particularly, the CV values that exceed 100% for January, February, July, August, November and December show that rainfall has an exceptionally high inter-annual variability due to $CV > 70\%$ for both scenarios (Figure 15).

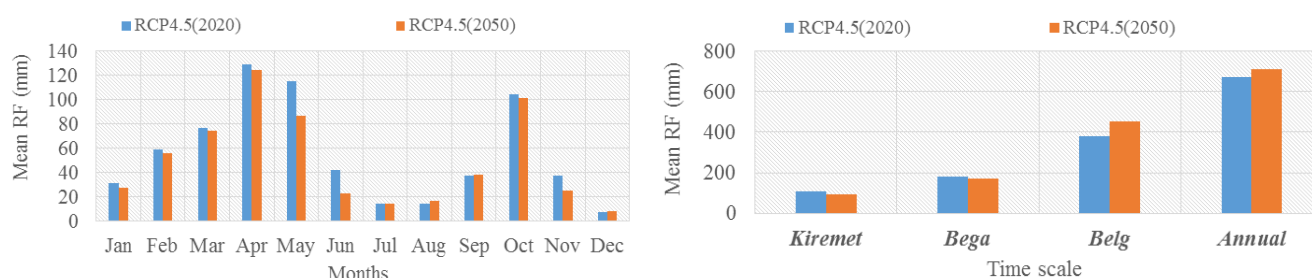


Figure 15. Mean monthly, Seasonal and Annual rainfall in the study area.

The amount of rainfall varies seasonally and geographically throughout the area. The seasonal distribution of rainfall reveals that *Belg* (February to May), which recorded a mean rainfall of 386.3mm, is followed by *Bega* (October to January), which experienced a mean record of 182.8 mm. However, *Kiremt* (June to September) was the period for the next 2020 with 107.8mm (Figure 16). As a result, there are three different seasons in the study area, and the rainfall that occurs throughout these seasons had brought on by south-easterly winds delivering moisture from the Indian Ocean. On the other hand, despite. *Arfasa* season (33.8%) has a significant variability of rainfall, while *Ganna* (64.7%) and *Bona* (47.5%) have higher variability. *Ganna* season followed by *Bona* was the lowest/driest season in the study area and rainfall is highly variable during *Ganna* exhibited the highest coefficient of variation respectively. The Mann-Kendall (MK) statistical test shows a statistically significant trend during the *Arfasa* season for both scenarios.

The second rainy season in Ethiopia is known as the *Belg*. The western and southern regions of the country receive more than 300mm of seasonal total rainfall, whereas the rest of the country has dry conditions [20]. From 2021 and 2050, the study region experienced a mean annual rainfall of 676.9 mm, with the peak rainfall occurring in 2038 (1220.8 mm). In 2027 (1120.3 mm) and in 2043 came next (965.4 mm). On the other hand, 2034, with 330 mm annually, was the lowest one. Throughout the examined period, there was somewhat high variable rainfall with a 31.4% coefficient of variation (Figure 16) for RCP4.5 (2020). Rainfall is highly variable, with a computed CV value of 37.3% on an annual basis, while the coefficient of variation for all month's spans between 37.7 to 293.7% for RCP8.5 (2020) and the computed CV value of 45.5% is very high rainfall variability and coefficient of variation for all months' spans between 29.1 to 256.1 for RCP8.5 (2050).

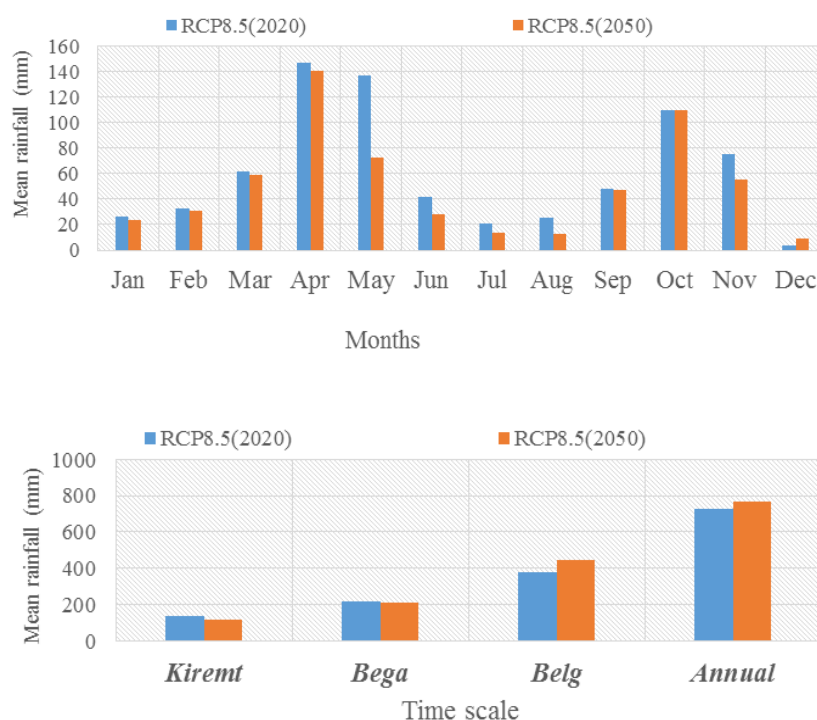


Figure 16. Monthly, Seasonal and Annual rainfall distribution in the study area (2021-2080).

3.6. Variability and Trends of Monthly, Seasonal and Annual Maximum and Minimum Observed Temperature

According to the mean T_{max} data, the highest month was February (32.4 °C), which was followed by January (29.9 °C) and March (29.8 °C), while the lowest mean T_{max} was recorded in July (23 °C). T_{max} exhibits a significant upward trend at the 5% level of significance (P-value 0.05). In the research

area, every month displays an upward trend (Figure 17). On the other side, for the entire period, February had the highest mean T_{min} (16.2 °C), followed by March (15.9 °C). Aside from this, July had the lowest mean T_{min} (13.9 °C). The MK test result showed that T_{min} had a significant increasing positive trend (P-value 0.05) in March, April, May, June, July, August, September, October, and November, with a change in magnitude that was roughly comparable (Figure 17).

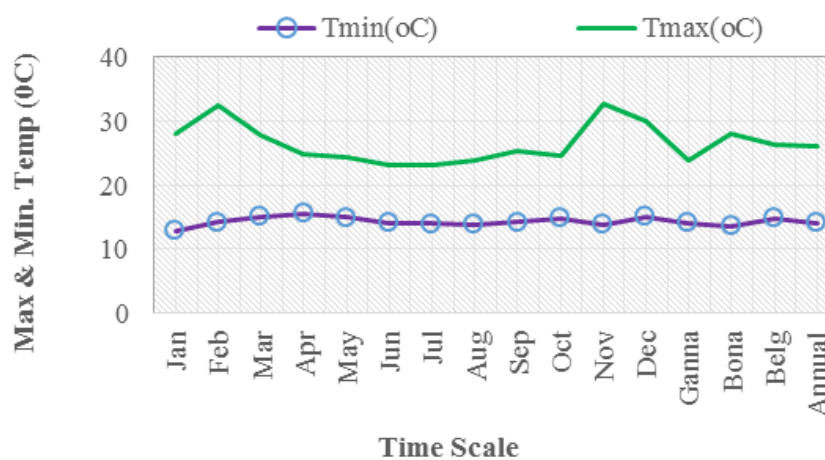


Figure 17. Mean monthly T_{max} and T_{min} in the study area (1991-2020).

3.7. Variability and Trends of Monthly, Seasonal and Annual Predicted Maximum Temperature

Figure 18 for mean T_{\max} shows that February was the highest month (29.4 °C) followed by January (29 °C) and March (28.5 °C) whereas the minimum mean T_{\max} was observed during July (24.2 °C) for RCP4.5 (2020) (Figure 18). On the other hand, the highest mean T_{\max} for RCP4.5 (2050) was observed in February (30 °C) followed by January (29.6 °C) during the entire period. Apart from this, the lowest mean T_{\max} was estimated in June (24.8 °C). The MK test result revealed all months have shown a significant increasing trend (P -value < 0.05) except in October for RCP4.5 (2050). The increase in the next months showed a monotonic trend. The results for mean T_{\max} show that February was the largest (30.8 °C) followed by January (29.9 °C) and March (29.8 °C) whereas the lowest mean T_{\max} was observed during July (26.4 °C) for RCP8.5 (2020) (Figure 18). On the other hand,

the highest mean T_{\max} for RCP8.5 (2050) was observed in February (31.7 °C) followed by January (30.8 °C) during the entire period. Apart from this, the lowest mean T_{\max} was recorded in July (26.4 °C). The MK test result revealed that all months have shown a significant increasing trend (P -value < 0.05) for both RCP8.5 scenarios. An increasing monotonic trend was detected during the rest of the months. *Bona* (winter) is the season with the most warmth in the research area is mean T_{\max} of 27.5 °C and 28.5 °C whereas *Ganna* (summer) is characterized by a relatively lowest mean of 25 °C and 25.8 °C for RCP4.5 (2020) and RCP4.5 (2050) respectively. Similarly, the mean T_{\max} for RCP8.5 (2020) and RCP8.5 (2050) for *Bona* was 28 and 29 °C respectively and for *Ganna* 25.5 and 27 °C respectively. The mean T_{\max} observed is relatively the highest and followed by *Birra* were (27.3 and 28.2 °C) for RCP4.5 (2020) and RCP4.5 (2050) respectively and for RCP8.5 (2020) and RCP8.5 (2050) was (27.6 and 28.5 °C) respectively as shown in Figure 18.

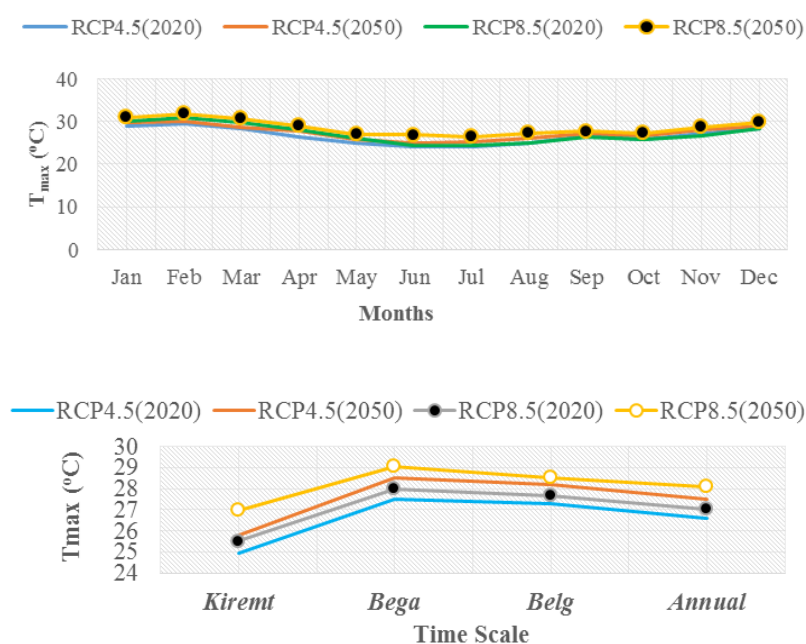


Figure 18. Mean monthly T_{\max} in Yabello station (2021-2080).

3.8. Variability and Trends of Monthly, Seasonal and Annual Predicted Minimum Temperature

The results for mean T_{\min} show that February was the highest month (16 °C) followed by March (15.8 °C) whereas, the lowest mean T_{\min} was observed during July (14 °C) for RCP4.5 (2020). T_{\min} demonstrates a strong upward trend (P value 0.05) at a 5% level of significance. All months show an increasing trend in the study area (Figure 19). On the other

hand, the highest mean T_{\min} for RCP4.5 (2050) was observed in February (16.4 °C) followed by March (16.3 °C) for the full-time period. In addition, the lowest mean T_{\min} value was noted in June (14.3 °C). The MK test result revealed all months have shown a significant increasing trend (P -value<0.05) except in October for RCP4.5 (2050). The results for mean T_{\min} show that February was the highest month (16.7 °C) followed by January (16.6 °C) whereas the lowest mean T_{\min} was observed during June (14.8 °C) for RCP8.5 (2020). T_{\min} shows a significant increasing trend (P -value<0.05) at a 5% level of significance. All months show an increasing trend in the study area. On the other hand,

the highest mean T_{\min} for RCP8.5 (2050) was observed in February (19.3 °C) followed by January (17.2 °C) for the full period. In addition, the lowest mean T_{\min} was noted in June (14.7 °C). The MK test result revealed that all months have shown a significant increasing trend ($P_{\text{value}} < 0.05$) for RCP8.5 (2050).

The study area's warmest season, *Bega* (*Bona*), has a mean T_{\min} of 15.5 °C and 15.9 °C whereas *Ganna* (*Kiremt*) is characterized by a relatively lowest mean of 14.9 °C and 15.3 °C

for RCP4.5 (2020) and RCP4.5 (2050) respectively. Similarly, the mean T_{\min} for RCP8.5 (2020) and RCP8.5 (2050) for *Bona* was 16.3 and 16.8 °C respectively and for *Ganna* 15.7 and 15.8 °C respectively. The mean T_{\min} observed is relatively the highest and followed by *Belg* (*Arfasa*) were (14.8 and 15.3 °C) for RCP4.5 (2020) and RCP4.5 (2050) respectively and for RCP8.5 (2020) and RCP8.5 (2050) was (15.4 and 16.4 °C) respectively as shown in Figure 19.

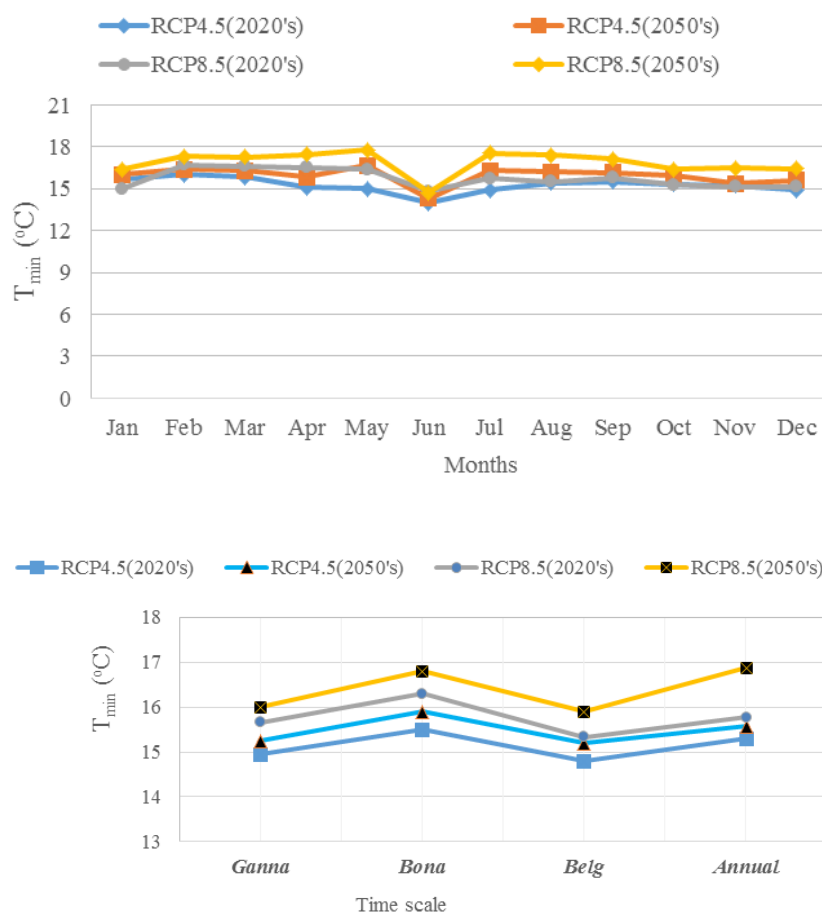


Figure 19. Mean monthly T_{\min} in Yabello station.

3.9. Comparison of Predicted Maximum and Minimum Temperature with the Baseline Period of RCP4.5 and RCP8.5

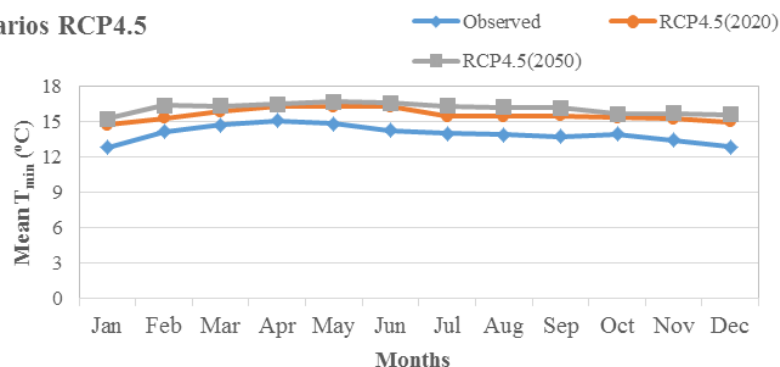
By using bias-corrected, future climate data, the temperature was calculated for the base period and the future climatic scenarios periods 2020 and 2050 (Figures 20 & 21). The outcome reveals that for the T_{\max} , baseline period, RCP4.5 (2020) and 2050 respectively fluctuate in the range of 22.5 to 28.2, 24.07 to 29.43 and 24.84 to 29.68 °C/month. As well as T_{\max} RCP8.5 (2020) and 2050 was 24.23 to 29.83 and 26.44 to 30.8 °C/month. Similarly, T_{\min} RCP4.5 (2020) and 2050 respectively range from 12.78 to 15.06, 14.79 to 16.6, and

16.36 to 17.77 °C/month, and T_{\min} RCP8.5 (2020) and 2050 range from 14.66 to 16.28 and 15.23 to 16.25 °C/month. The T_{\max} steadily rises until it reaches its peak value in February is around 28.2 °C/month for the base period, 29.43 °C/month for RCP4.5 (2020), and 29.68 °C/month for RCP4.5 (2050). Moreover, T_{\max} peaks at 29.83 for RCP8.5 (2020) and 30.74 °C/month for RCP8.5 (2050) in the same months. Then, for the base period, RCP4.5 (2020), and 2050, respectively, in June month, and for the base period, RCP8.5 (2020), and 2050, respectively, in July months, its minimum value is 22.4, 24.04, and 24.84 °C/month and 24.23 °C/month and 26.44. This finding is similar to those reported by [22]. Similar to how T_{\min} rises gradually, it reaches its peak values in April, March, and May of the following values 15.06 °C for the base

period, 16.6 °C for RCP4.5 (2020), and 17.77 °C for RCP4.5 (2050). Moreover, T_{min} with peak values in April of 16.28 for RCP8.5 (2020) and 16.43 °C/month for RCP8.5 (2050). Then,

for the base period, RCP4.5 (2020), RCP4.5 (2050), RCP8.5 (2020), and RCP8.5 (2050), respectively, its minimum value is 12.78, 14.79, 16.39, 14.66 and 15.23 °C/month.

Scenarios RCP4.5



Scenarios RCP8.5

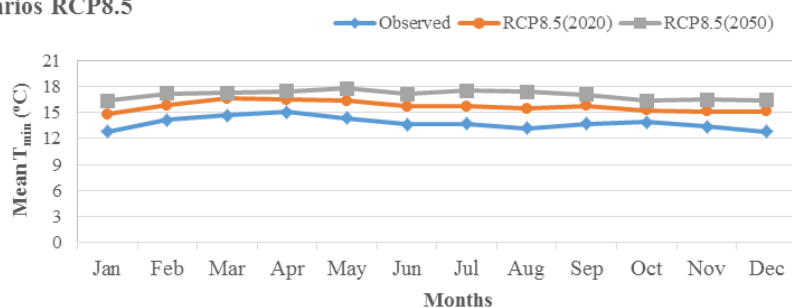
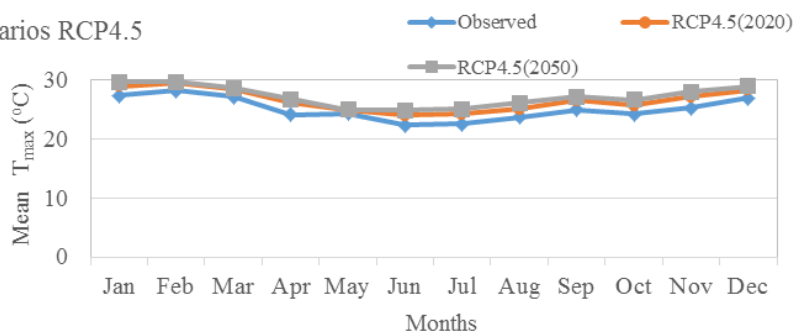


Figure 20. Minimum temperature at base period, the 2020s and 2050s scenarios periods.

Scenarios RCP4.5



Scenarios RCP8.5

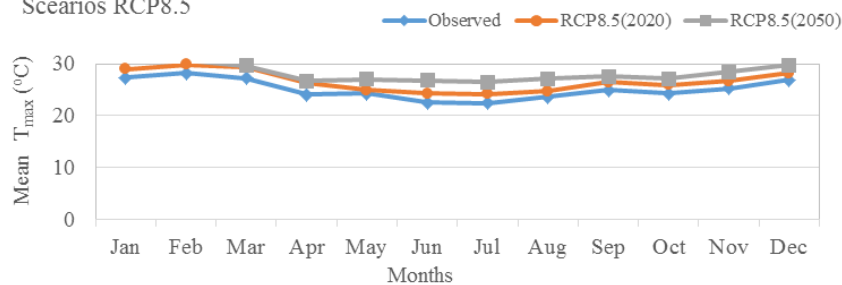


Figure 21. Maximum temperature at base period, the 2020s and 2050s scenarios periods.

3.10. Monthly and Seasonal Projected Rainfall

The percentage change of mean monthly and annual rainfall is shown in this section for two scenarios and time horizons of RCP 4.5 (2020) and RCP 8.5 (2050) scenarios. The Power Transformation of the precipitation method was used to rectify the biases in the scenario data for RCP 4.5 and 8.5 based on the criteria of goodness of fit tests. After that, they were divided into two periods the 2020s (2025-2054) and 2050s (2055-2084). The mean monthly rainfall scenarios in 2020 and 2050 under RCP 4.5 and RCP 8.5 are shown in Figure 22. Monthly mean rainfall in the RCP 4.5 (2020) showed a reduction in January, Feb, March, April, May, June, July, August, September, November and December, while it increased in March, September and October for different scenarios Figure 22. January and November were the months with the greatest decrement with values of 38.49% and 35.63% for RCP8.5 (2050) and RCP4.5 (2050) respectively. March and October are also the months with the greatest

increment with values of 15.52% and 28.41% for RCP 8.5 (2050) and RCP4.5 (2020) respectively.

The 2020 RCP 4.5 mean rainfall also decreased and increased in the months of that RCP's (2050) except for March and October. The reduction in mean rainfall ranged from -0.1% to -31.44%, while the increment in mean rainfall ranged to +28.41% for RCP4.5 (2020) and the decrement ranges from -1.06% to -35.63% and the increment ranges from +5.81 to +11.73% respectively for RCP4.5 (2050). In addition, the mean rainfall decrement -0.47% to -35.05% and the increment was +16.86% for RCP8.5 (2020) and the mean rainfall decrement -1.2% to -38.49% and the increment was +15.52% to +25.51% RCP8.5 (2050) respectively. March shows the smallest increment and May shows the smallest decrement with values of 5.81% in RCP 4.5 (2050) and -0.1% in RCP 4.5 (2020) respectively. The same result for October was the highest increment and decrement was January with a value of +28.41% for RCP4.5 (2020) and -38.49% for RCP8.5 (2050) respectively.

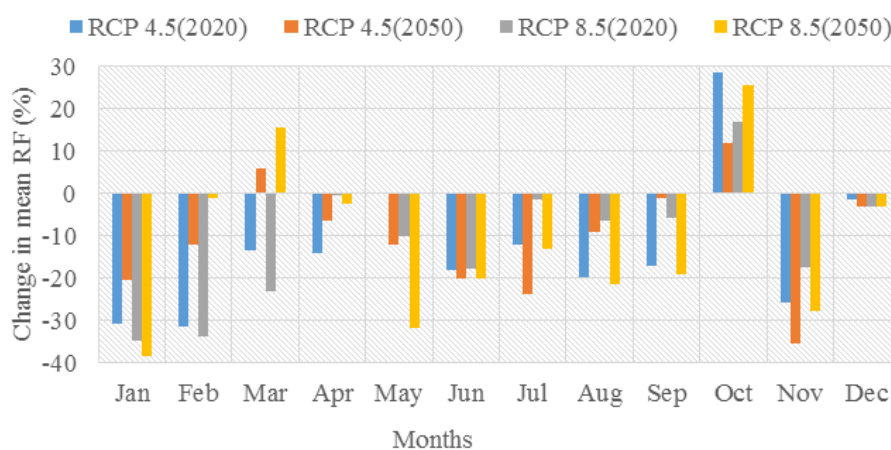


Figure 22. Monthly percent changes in rainfall under both scenarios and periods.

Furthermore, the RCP 8.5 forecast for the 2020s showed a drop in mean rainfall in the months of all except October months. In addition, the 2050 RCP 8.5 simulation revealed a rise in March and October and a drop in the rest of the months. In October and January, respectively, the greatest increment and decline were seen. According to the findings, there is a decreased pattern in precipitation change for both scenarios and future periods, and the change fluctuates from month to month except for March and October. This result is in agreement with the findings of [9]. The "Bega/Bona" season one of three displayed in the study areas. It is characterized by periods of sunny, dry weather mixed with sporadic falls or irregular/random from October until January. On the other hand, under typical circumstances, the southern and southeastern lowlands only see a brief rainy season. The "Arfasa" small rainy season, which lasts from February to May and covers the southern, central, eastern, and northeastern parts of the country. "Kiremt/Ganna" main rainy season,

which lasts from June to September for most of the country except for the southeastern lowlands, causes cooler mornings and nights and warmer days during the season [12, 1]. As shown in Figure 23, the Ganna and Bona seasons showed that there is a decreasing change in precipitation for both scenarios along with two time horizons from the base periods except for the Belg season. The precipitation changes in the Ganna season ranged from -11.56% to -25.55%, with RCP8.5 (2020) revealing the greatest decrease and RCP 4.5 (2050) the smallest. About -14.15% to -23.48% change in Bona precipitation was detected in the relatively minimum decrement estimated in RCP 4.5 (2020) and the maximum observed in RCP 8.5 (2050).

Furthermore, in both scenarios, Belg seasons exhibited an increment trend in study areas. It changes by approximately +7.47% to +16.38%. The greatest growth change was found under RCP8.5 (2020), while the lowest was in RCP4.5 (2020). According to these findings, the Belg seasons were

expected to face medium precipitation and the *Ganna* and *Bona* seasons were expected to face lower precipitation changes. These findings are consistent results with those reported by [19]. According to [6, 36] Forecasts for precipitation are less certain than forecasts for temperatures and more spa-

tially, and seasonally dependent than temperature projections. According to [16], Global temperature increases of $\sim 4^{\circ}\text{C}$ or more above late 20th century levels combined with increasing food demand, would pose large risks to food security globally with high confidence.

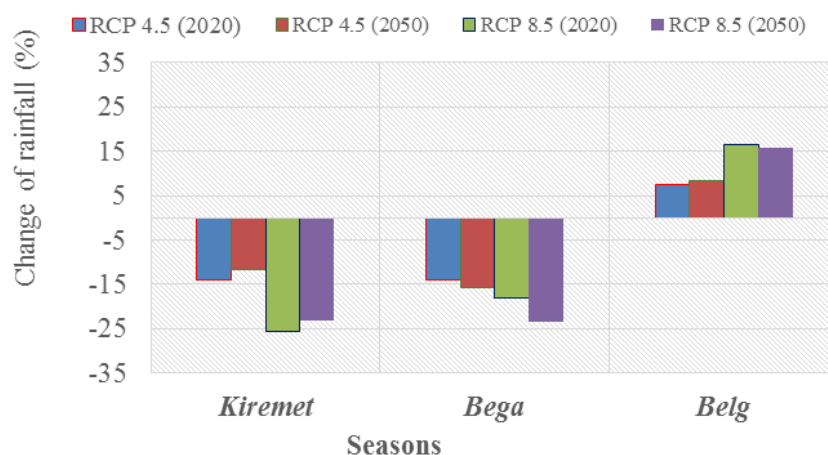


Figure 23. Seasonal projected change of rainfall from the base period.

3.11. Projected Annual Rainfall

Figure 24 shows the percentage change in mean annual rainfall for RCP4.5 (2020), RCP4.5 (2050), RCP8.5 (2020), and RCP8.5 (2050). From the annual rainfall analysis, the results revealed a decreasing trend from base periods through both the RCP 4.5 and RCP 8.5 scenarios for each period. There is a -9.5% and -8.45% decrease in mean annual rainfall from the base periods to RCP4.5 (2020) and RCP4.5 (2050) respectively, and about -10.5% and -10.95% in RCP8.5

(2020) and RCP8.5 (2050) respectively. Generally, in this work, Five GCM-RCM (CanESM2, EC-EARTH, HadGEM2-ES, MIROC5, and MPI-ESM-MR) driven by the RCP4.5 and RCP8.5 emission scenarios were selected to project the future precipitation. Considering the ensemble mean of five GCMs, the future changes in precipitation concerning the baseline period were presented. These findings are consistent with those reported by [21]. According to these findings, in the stations under study, yearly rainfall shows a trend toward decline.

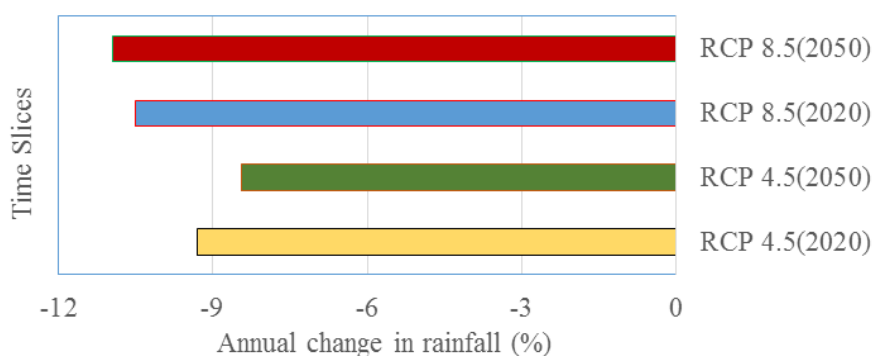


Figure 24. Projected percentage change in annual rainfall from the baseline period.

3.12. Projected Monthly, Seasonal and Annual Maximum Temperature

The mean monthly, seasonal and annual temperature exhib-

its distinct upward trends for almost all months, seasons and years, as well as for both periods. Figure 25 shows the change in mean monthly maximum temperature in the 2020 and 2050 periods under RCP4.5 and RCP8.5. In 2020, the RCP4.5 simulations revealed a 2.3°C to 2.7°C increase in mean maximum

temperature. February shows the most significant increase, whereas July shows a much smaller increase. The RCP4.5 (2050) also showed an increase from the baseline period in all months. The simulation suggested an increase in the range of 2.59 °C to 3.4 °C with the maximum increase projected in February and the minimum observed in July. Also, both RCP8.5 (2020) and RCP8.5 (2050) simulations showed a rise in the mean maximum temperature with values of 2.6 °C to 2.93 °C and 2.8 °C to 3.5 °C, respectively. The largest change was simulated in October, whereas the smallest was simulated in July under RCP8.5 (2020), and the highest and the lowest increases were detected in February and July under RCP8.5 (2050), respectively. In terms of the mean annual maximum temperature the change in mean annual maximum temperature under RCP4.5 (2020) and RCP4.5 (2050) ranges from 2.61 °C to 2.83 °C, with the highest change predicted for RCP4.5 (2050's)

and the lower reported for RCP4.5 (2020). While its values range from 2.71 °C to 3.36 °C under RCP8.5, the largest was found under RCP8.5 (2050) and the smallest was found under RCP8.5 (2020) respectively [7, 17] found similar results. According to [17], the average temperature in Ethiopia will climb by 0.8 °C in the 2020s and 1.2 °C in the 2050s. It also predicted that relative to 1961 to 1999, the average temperature change in Ethiopia's central region would be in the range of 1.0 °C to 1.1 °C by 2020s and in the range of 1.82 °C by the 2050s. This result is in agreement with the findings of [25]. According to this conclusion increase of global mean surface temperatures for 2081–2100 relative to 1986–2005 is projected to likely be in the ranges derived from the concentration-driven CMIP5 model simulations, that is, 1.1 °C to 2.6 °C for RCP4.5, and 2.6 °C to 4.8 °C for RCP8.5.

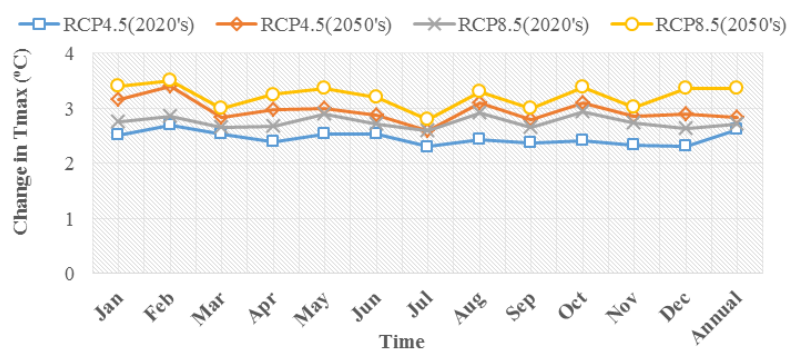


Figure 25. Change in mean monthly and annual T_{max} from baseline period to future scenarios.

All Kiremet, Bega, and Belg seasons indicate a growing change from the base period through both RCP4.5 and RCP8.5 across time horizons as shown in Figure 26. Ganna's mean maximum temperature variations in both scenarios revealed an increase from the baseline periods across both time horizons. The greatest change (3.45 °C) was seen in RCP8.5 (2050), and the smallest (2.22 °C) was obtained in RCP4.5 (2020). In both periods, a maximum temperature change of about 2.55 °C to 3.45 °C was obtained throughout the Bona seasons in both scenarios. RCP8.5 (2050) had the biggest temperature change whereas RCP4.5 (2020) had the

lowest. Moreover, the maximum temperature change ranged from 2.37 °C to 3.23 °C in the Belg season, in which the highest change was observed in RCP8.5 (2050) and the lowest obtained in RCP4.5 (2020) respectively. According to the [16], Global temperature increases of ~4 °C or more above late 20th century levels combined with increasing food demand, would pose large risks to food security globally with high confidence. In comparison to a baseline, it anticipated that climate change resulted in a rise in poor health across many regions of the 21st century, particularly in low-income developing nations without climate change.

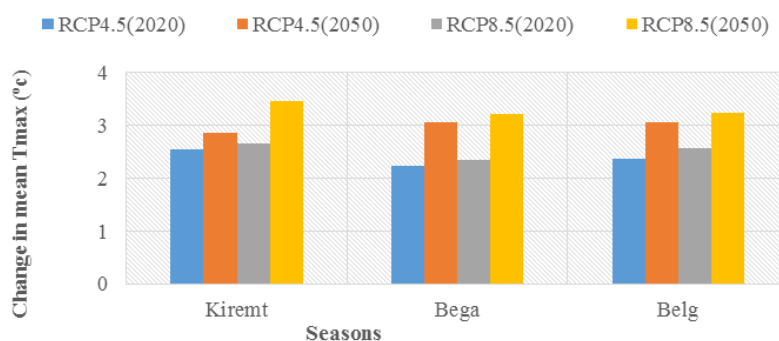


Figure 26. Mean seasonal change of maximum temperature from the baseline period.

3.13. Projected Monthly, Seasonal and Annual Minimum Temperature

Figure 27 illustrates the change in mean monthly minimum temperature under RCP4.5 in 2020 and 2050 compared to the baseline period. All months for both scenario simulations showed an increase in mean minimum temperature. In all months of both periods, simulations demonstrated an increase in the mean minimum temperature with temperature differences changes ranging from 2.1 °C to 2.8 °C, 2.6 °C to 3.3 °C, 2.41 °C to 3.16 °C and 3.1 °C to 3.39 °C for RCP4.5 (2020), RCP4.5 (2050), RCP8.5 (2020) and RCP8.5 (2050) respectively. The biggest increase was in October and November and the lowest was in March for RCP4.5 (2020). The RCP4.5 (2050) simulation also showed an increase in mean minimum temperature. The range of increase in mean minimum temperature was from 2.6 °C to 3.3 °C. Furthermore, during RCP8.5 (2020) scenarios, there is an increase in the mean minimum temperature, with changes ranging from 2.41 °C to 3.16 °C in all months. In February, the largest change was simulated, and in March, was the smallest. In general, for all months there is an increasing trend for both mean monthly maximum and minimum temperatures from the base period to both RCP4.5 and 8.5 scenarios. For both the 2020s and 2050s periods, maximum and minimum temperatures are increasing from the base period to the high emission (RCP8.5) scenarios than the medium emission (RCP4.5) scenario since RCP8.5 has higher greenhouse gas emissions than the RCP4.5 scenarios [25]. Regarding the mean annual minimum temperature (Figure 27),

the change in mean annual minimum temperature ranges from 2.94 °C to 3.45 °C between RCP4.5 (2020) and RCP4.5 (2050), with the higher change occurring under RCP4.5 (2050) and the lower occurring under RCP4.5 (2020). While it ranges from 3.21 °C to 3.59 °C under RCP8.5, the largest found under RCP8.5 (2050) and the smallest discovered under RCP8.5 (2020). According to [11], average annual maximum and minimum temperatures significantly increase in both future periods and RCPs scenarios over the Upper Blue Nile River basin. The result is also consistent with [4, 33]. According to this conclusion, RCP4.5 predicts a 1.6 °C to 2 °C increase in maximum temperature and a 1.8 °C to 2.4 °C increase in minimum temperature between the mid and end of the century, respectively. Similarly, RCP8.5 anticipates a 2.1 °C and 3.7 °C increase in maximum temperature and a 2.6 °C and 4.6 °C increase in minimum temperature between the mid and end of the century, respectively. In general, from the base period to both the RCP4.5 and RCP8.5 scenarios, there is an increasing pattern for the monthly and yearly minimum temperatures. According to [16] Without additional efforts to reduce GHG emissions beyond those in place today, global emissions growth is expected to persist, driven by growth in global population and economic activities. Global mean surface temperature increases in 2100 in baseline scenarios those without additional mitigation range from 3.7 °C to 4.8 °C above the average for 1850–1900 for a median climate response. They range from 2.5 °C to 7.8 °C when including climate uncertainty (5th to 95th percentile range) with a high confidence level.

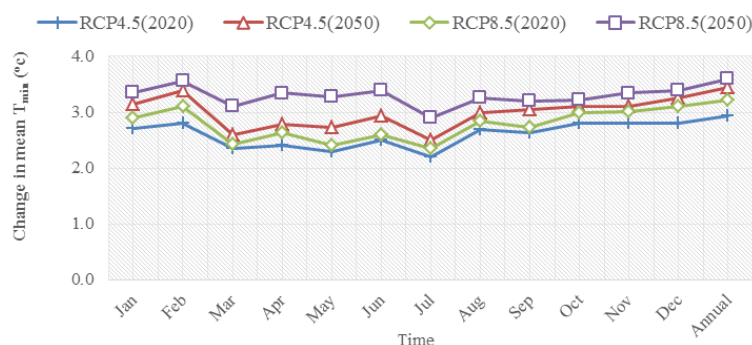


Figure 27. Change in mean monthly and annual min. temperature under future climate change.

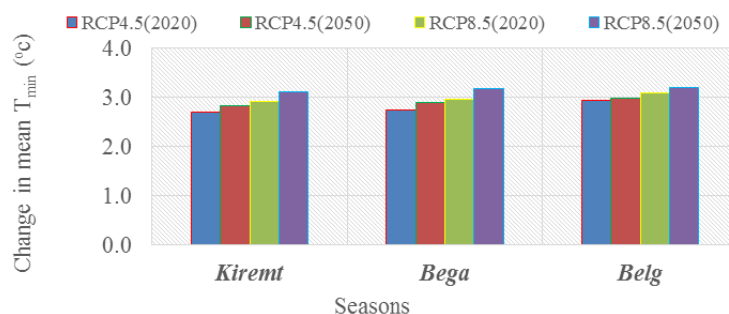


Figure 28. Mean change of minimum temperature from the baseline period.

Ganna (Kiremet), *Bona (Bega)* and *Birra (Belg)* season minimum temperatures exhibit an increasing shift from the base period in all time horizons for both RCP4.5 and RCP8.5, as depicted in Figure 28. Across all time horizons, the *Ganna* minimum temperature change in both scenarios showed an increase from the baseline period. RCP8.5 (2050) had the biggest (3.2 °C) shift whereas RCP4.5 (2020) had the smallest (2.71 °C). During the *Bona* season, both scenarios achieved a minimum temperature change of roughly 2.75 °C to 3.19 °C using both periods. The greatest temperature change was projected in RCP8.5 (2050), whereas the smallest was in RCP4.5 (2020). Furthermore, throughout the *Belg* season, the minimum temperature change ranged from 3.93 °C to 3.2 °C, with the biggest change likely occurring in RCP8.5 (2050) and the lowest in RCP4.5 (2020). The result is inconsistent with the finding of Tessema *et al.*, 2017a and [2].

4. Conclusions

According to the study, the percentage change reduction in mean monthly rainfall ranged from 0.1% to 31.44% where the maximum observed in January and the minimum detected in May under RCP 4.5 (2020). The increment in mean rainfall was 28.41%, which was the maximum observed in October under RCP 4.5 (2020). Decrement ranges from -1.06% to -35.63% the maximum observed in November and the minimum detected in September and increment ranges from +5.81 to +11.73% where the maximum was observed in October and the minimum was detected in March respectively under RCP 4.5 (2050). In this study, the average monthly rainfall decreased by a percentage ranging from -0.47% to -35.05%, with the maximum observed in January and the minimum detected in April. The average monthly rainfall increased by a percentage of +16.86 with the maximum observed in October under RCP 8.5 (2020) and the decrement under RCP 8.5 (2050) spans from -1.2% to -38.49%, with the maximum recorded in January and the minimum identified in February. The increment for RCP8.5 (2050) is between +15.52% and +25.51%, with the largest increment being seen in October and the minimum increase being discovered in March. Seasonal rainfall shown decreasing in all scenarios and periods by *Kiremet* and *Bega*, ranges between -11.56% to -25.55% and -14.15% to -23.48%, respectively. The maximum and minimum decrements were seen in *Kiremet* at RCP8.5 (2020) and RCP4.5 (2050), respectively, while they were shown in *Bega* at RCP8.5 (2050) and RCP4.5 (2020). With a range value of 7.47% to 16.38%, rainfall during the *Belg* season increased relative to the base period. Additionally, the range of annual rainfall decreases from the base period in all scenarios was -11.56% to -25.55%, with the largest decline occurring in RCP8.5 (2020) and the minimum decline occurring in RCP4.5 (2050).

Based on the result of the future scenarios of maximum and

minimum temperature, the study also discovered that the RCP4.5 (2020) scenarios anticipated a 2.3 °C to 2.7 °C increase in mean maximum temperature, with February having the largest change and July having the smallest. In the 2050s with RCP4.5 scenarios, the range of the mean maximum temperature was 2.59 °C to 3.4 °C in which the maximum increase was detected in the same months RCP4.5 (2020). The mean maximum temperature increased by 2.6 °C to 2.93 °C and 2.8 °C to 3.5 °C in RCP8.5 (2020) and (2050), respectively. All months showed an increasing trend in maximum temperature from the base period to RCP4.5 and RCP8.5, with a maximum of 3.5 °C obtained under RCP8.5 (2050) and a minimum change of 2.3 °C observed under RCP4.5 (2020). Seasonally, maximum and minimum temperatures also discovered that the RCP4.5 (2020) and RCP4.5 (2050) scenarios anticipated a 2.22 °C to 2.85 °C and 2.55 °C to 3.05 °C increase in mean maximum temperature respectively for *Ganna* season having the smallest and *Bona* having the largest change. In the 2050s with RCP4.5 scenarios, the mean maximum temperature was highest, in which the maximum increase was detected. The mean maximum temperature increased by 2.37 °C to 3.04 °C and 2.56 °C to 3.23 °C in RCP4.5 and RCP8.5, respectively. All seasons showed an increasing trend in maximum temperature from the base period to RCP4.5 and RCP8.5, with a maximum of 3.45 °C obtained under RCP8.5 (2050) and a minimum change of 2.22 °C observed under RCP4.5 (2020). Annually, the change in mean maximum temperature increased in each scenario and time horizon from the observed period. The Simulation revealed that the highest and lowest 2.83 °C and 2.61 °C changes in the maximum temperature had been detected under RCP4.5 (2050) and (2020). The most significant increase occurred in RCP8.5 (2050) with a temperature change of +3.36 °C and +2.71 °C with the lowest in RCP4.5 (2020).

Moreover, the RCP4.5 (2020) scenarios indicated an increase in minimum temperature ranging from +2.1 °C to +2.8 °C, and the highest and lowest were recorded in February and July, respectively. In the 2050s with RCP4.5 scenarios, the range of the mean minimum temperature was 2.6 °C to 3.39 °C with which the maximum increase was detected in the same months RCP4.5 (2020). The mean minimum temperature had increased by 2.41 °C to 3.16 °C and 3.1 °C to 3.55 °C in RCP8.5 (2020) and (2050), respectively. All months showed an increasing trend in minimum temperature from the base period to RCP4.5 and RCP8.5, with a maximum of 3.55 °C obtained under RCP8.5 (2050) and a minimum shift of 2.2 °C observed under RCP4.5 (2020). The minimum temperature showed a rising shift from the base period in all *Belg*, *Kiremet*, and *Bega* seasons, with maximum and minimum of 2.72-3.2 °C, 2.71-3.1 °C, and 2.73-3.45 °C, respectively. Furthermore, the change of mean annual minimum ranged from 2.71 to 3.45 °C, in which the maximum was recorded under RCP8.5 (2050) and the lowest was recorded under RCP4.5 (2020). Annually, the change in mean minimum temperature increased in each scenario and time horizon from the

observed period. The Simulation revealed that the highest and lowest 3.59 °C and 2.94 °C of changes in the maximum detected under RCP8.5 (2050) and RCP4.5 (2020). The most significant increase occurred in RCP8.5 (2050) with a temperature change of +3.21 °C and +3.59 °C with the lowest in RCP4.5 (2020). Rainfall in study areas is highly variable, as indicated by the computed CV value of 34.45% on an observed annual basis and variability of rainfall for RCP4.5 (2020) and 2050, RCP8.5 (2020), and 2050 was 31.4%, 27%, 37.3 and 45.5% respectively. *Bega* is the warmest time of year in the research area, with a mean T_{max} of 27.5 °C and 28.5 °C whereas *Kiremet* is characterized by relatively lowest mean of 25 °C and 25.8 °C for RCP4.5 (2020) and RCP4.5 (2050) respectively. Similarly, the mean T_{max} for RCP8.5 (2020's) and RCP8.5 (2050 for *Bega* was 28 and 29 °C respectively, and for *Kiremet* 25.5 and 27 °C respectively. The mean T_{max} observed is relatively the highest and followed by *Belg* were (27.3 and 28.2 °C) for RCP4.5 (2020) and 2050 respectively and for RCP8.5 (2020) and 2050 was (27.6 and 28.5 °C) respectively. According to the study's findings, maximum and minimum temperatures was rise in the future due to the effects of climate change. So, various climate adaptation and mitigation methods like, developing training for the community to raise local understanding of climate change and its impacts, Participating national and international NGOs those focus on environmental issues, community should adopt soil and water conservation techniques, Implement various trees, apply a water harvesting structure and more multiple GCM-RCM driving models with various RCM outputs to improve more prediction accuracy in the future studies. In general this study is supposed to be a significant contribution for the public authority, society and strategy creators in executing environmental change transformation and relief programs in the Dawa watershed for the manageable use.

Abbreviations

CORDEX	Coordinated Regional Climate Downscaling Experiment
RCP	Representative Concentration Pathways
CMhyd	Climate model for Hydrology
HWSD	Harmonized World Soil Database
MoWE	Ministry of Water and Energy

Acknowledgments

The authors would like to thanks to Oromia Agricultural Research Institute for helping me with finance and giving me this scholarship and Mechara Agricultural Research Center for facilitating finance.

Author Contributions

Ayana Bulti: Conceptualization, Data curation, Formal Analysis, Investigation, Methodology, Software, Validation, Visualization, Writing – original draft, Writing – review &

editing

Fentaw Abegaz: Supervision, Validation, Visualization

Funding

This study was supported through funding from Oromia Agricultural Research Institute. The funding sponsor had no role in the design of the study in the analyses or interpretation of data; in the writing of the manuscript.

Data Availability Statement

The author's want to express utmost gratitude to the Ethiopia National Meteorological Agency for providing all required Meteorological data and the Ministry of Water and Energy of Ethiopia for providing essential Stream flow data.

Conflicts of Interest

The authors declare no conflicts of interest.

References

- [1] Abebe, D. (2010) 'Future climate of Ethiopia from PRECIS Regional Climate Model Experimental Design', (November).
- [2] Ademe, M., Eric, N. O. and Tesfaye, L. (2019), "Determinants of adaptation choices to climate change in agro-pastoral dry lands of northeastern Amhara, Ethiopia", *Cogent Environmental Science*, Vol. 5 No. 1, pp. 1, 23, <https://doi.org/10.1080/23311843.2019.1636548>
- [3] Aloysius, N. R., Sheffield, J., Saiers, J. E., Li, H. & Wood, E. F. 2016. Evaluation of historical and future simulations of precipitation and temperature in central Africa from CMIP5 climate models. *Journal of Geophysical Research: Atmospheres* 121 (1), 130–152.
- [4] Bekele Daniel, Tena Alamirew, Asfaw Kebede, Gete Zeleke & Assefa M. Melesse 2019 "Modeling Climate Change Impact on the Hydrology of Keleta Watershed in the Awash River Basin, Ethiopia," *Environmental Modeling and Assessment*, 24(1), pp. 95 107. <https://doi.org/10.1007/s10666-018-9619-1>
- [5] Boru, G. F. and Regassa, F. D. (2020) 'Impact of Climate Change on Irrigated Crop Water Use of Selected Major Grown Crops and Water Demand for Irrigation: a Case of Anger Sub-Basin, Nile Basin of Ethiopia', *International Journal of Engineering Applied Sciences and Technology*, 04(09), pp. 452–464. Available at: <https://doi.org/10.33564/ijeast.2020.v04i09.062>
- [6] David P. Rowell (2012) Sources of uncertainty in future changes in local precipitation. <https://doi.org/10.1007/s00382-011-1210-2>
- [7] Declan Conway, E. Lisa F. Schipper 2010. Adaptation to climate change in Africa: Challenges and opportunities identified from Ethiopia.

- [8] Duba, G. W., Demissie, S. T., & Emiru, T. S. (2021). Meteorological Droughts from 1987–2017 in Yabello and El-Woye Areas of Borana, Oromia Region, Ethiopia. *Ethiopian Journal of Social Sciences*, 7(1).
- [9] Enyew BD, Van Lanen HAJ and Van Loon AF 2014. Assessment of the Impact of Climate Change on Hydrological Drought in Lake Tana Catchment, Blue Nile Basin, Ethiopia. <http://dx.doi.org/10.4172/2329-6755.1000174>
- [10] Feng, S., Hu, Q., Huang, W., Ho, C. H., Li, R. & Tang, Z. 2014. Projected climate regime shift under future global warming from multi-model, multi-scenario CMIP5 simulations. *Global and Planetary Change* 112, 41–52.
- [11] Gebre, S. L. and Ludwig, F.: Hydrological response to climate change of the Upper Blue Nile River Basin: based on IPCC Fifth Assessment Report (AR5), *Journal of Climatology & Weather Forecasting*, 3, 121, <https://doi.org/10.4172/2332-2594.1000121>, 2015
- [12] Gebrie Geremew and Engida Agizew (2015) Climate Modeling of the Impact of Climate Change on Sugarcane and Cotton for Project on ‘a Climate Resilient Production of Cotton and Sugar in Ethiopia’ By Geremew Sahilu Gebrie (PhD) Addis Ababa, Ethiopia. Addis Ababa.
- [13] Gizaw, M. S., Biftu, G. F., Gan, T. Y., Moges, S. A. & Koi-vusalo, H. 2017 Potential impact of climate change on streamflow of major Ethiopian rivers. *Clim. Change* 143 (3–4), 371–383.
- [14] Gunavathi S (2021) ‘Assessment of Various Bias Correction Methods on Precipitation of Regional Climate Model and Future Projection’.
- [15] Hosseini, R. H., Golian, S. & Yazdi, J. 2020. Evaluation of data driven models to downscale rainfall parameters from global climate models outputs: the case study of Latyan watershed. *Journal of Water and Climate Change* 11 (1), 200–216. <https://doi.org/10.2166/wcc.2018.191>
- [16] IPCC, 2014 (2014) Climate Change 2014 Synthesis Report.
- [17] Menale Kassie, Moti Jaleta, Bekele Shiferaw, Frank Mmbando, Mulugetta Mekuria 2013. Adoption of interrelated sustainable agricultural practices in smallholder systems: Evidence from rural Tanzania.
- [18] Mirdashtvan, M., Najafinejad, A., Malekian, A. & Sa’doddin, A. 2018. Downscaling the contribution to uncertainty in climate change assessments: representative concentration pathway (RCP) scenarios for the South Alborz Range, Iran. *Meteorological Applications* 25 (3), 414–422.
- [19] National meteorological Agency, (NMA) (2005) ‘National meteorological services agency agrometeorological bulletin seasonal agro meteorological bulletin’, 15(3), pp. 1–19.
- [20] NMA (2022) Climate Diagnostic Bulletin of Belg (February to May) 2022. Addis Ababa.
- [21] Phillips, T. J., Bonfils, C. J. & Zhang, C. 2019. Model consensus projections of US regional hydro climates under greenhouse warming. *Environmental Research Letters* 14 (1), 014005.
- [22] Reddy, P. (2015) Climate Resilient Agriculture for Ensuring Food Security. Karnataka: springer New Delhi Heidelberg New York Dordrecht London. Available at: <https://doi.org/10.1007/978-81-322-2199-9>
- [23] Richard H. Moss, Jae A. Edmonds, Kathy A. Hibbard, Martin R. Manning, Steven K. Rose, Detlef P. van Vuuren, Timothy R. Carter, Seita Emori, Mikiko Kainuma, Tom Kram, Gerald A. Meeh, John F. B. Mitche, Nebojsa Nakicenovic, Keywan Riahi, Steven J. Smith, Ronald J. Stouffer, Allison M. Thomson, John P. Weyant & Thomas J. Wilbanks 2010 “The next generation of scenarios for climate change research and assessment,” *Nature*, 463(7282), pp. 747–756. <https://doi.org/10.1038/nature08823>
- [24] Sabeerali, C. T., Ramu Dandi, A., Dhakate, A., Salunke, K., Mahapatra, S. & Rao, S. A. 3013. Simulation of boreal summer intraseasonal oscillations in the latest CMIP5 coupled GCMs. *Journal of Geophysical Research: Atmospheres* 118 (10), 4401–4420.
- [25] Stocker, T. F., D. Qin, G. K. Platter, M. Tignor, S. K. Allen, J. Boschung, A., Nauels, Y. Xia, V. e. and P. M. M. (2013) ‘Climate change 2013: The physical science basis, in contribution of Working Group I (WGI) to the Fifth Assessment Report (AR5) of the Intergovernmental Panel on Climate Change (IPC...’, (September 2014).
- [26] Tegemeo Institute, E. U. 2011 Proceedings of the Workshop on Climate Change and Rural Livelihoods Held on February 3, 2011 Fairview Hotel, Nairobi.
- [27] Thomas, T., Goyal, S., Goyal, V. C. & Kale, R. V. 2018 Water availability under changing climate scenario in Ur river basin. In: *Climate Change Impacts*. Springer, Singapore, pp. 213–229.
- [28] Ullah, A., Ahmad, I., Ahmad, A., Khaliq, T., Saeed, U., Habib-ur Rahman, M., Hussain, J., Ullah, S. & Hoogenboom, G. 2019. Assessing climate change impacts on pearl millet under arid and semi-arid environments using CSM-CERES-Millet model. *Environmental Science and Pollution Research* 26 (7), 6745–6757.
- [29] Warnatzsch, E. A. & Reay, D. S. 2019 Temperature and precipitation change in Malawi: evaluation of CORDEX-Africa climate simulations for climate change impact assessments and adaptation planning. *Science of the Total Environment* 654, 378–392.
- [30] Worku, M. A., Feyisa, G. L. and Beketie, K. T. (2022a) ‘Climate trend analysis for a semi-arid Borana zone in southern Ethiopia during 1981–2018’, *Environmental Systems Research*, 11(1). Available at: <https://doi.org/10.1186/s40068-022-00247-7>
- [31] WWAP/UN-Water 2018. The United Nations World Water Development Report 2018: Nature-Based Solutions for Water. UNESCO, Paris.
- [32] Xinyi. Li and Zhong. Li (2023) ‘Evaluation of bias correction techniques for generating high - resolution daily temperature projections from CMIP6 models’, *Climate Dynamics*, 61(7), pp. 3893–3910. Available at: <https://doi.org/10.1007/s00382-023-06778-8>

- [33] Yadeta, D., Kebede, A. and Tessema, N. (2020) 'Climate change posed agricultural drought and potential of rainy season for effective agricultural water management, Kesem sub-basin, Awash Basin, Ethiopia', *Theoretical and Applied Climatology*, 140(1–2), pp. 653–666. Available at: <https://doi.org/10.1007/s00704-020-03113-7>
- [34] Yang, Y., Bai, L., Wang, B., Wu, J. & Fu, S. 2019 Reliability of the global climate models during 1961–1999 in arid and semiarid regions of China. *Science of the Total Environment* 667, 271–286.
- [35] Zarghami, M., Abdi, A., Babaeian, I., Hassanzadeh, Y. & Kani, R. 2011. Impacts of climate change on runoffs in East Azerbaijan, Iran. *Global and Planetary Change* 78 (3–4), 137–146.
- [36] Kebede, A. (2013) Downscaling Climate Model Outputs for Estimating the Impact of Climate Change on Water Availability over the Baro-Akobo River Basin, Ethiopia. Doctoral Dissertation, Bonn University, Germany.
- [37] Ebrahim, G. Y., Jonoski, A., Van Griensven, A., & Di Baldassarre, G. (2013). Downscaling technique uncertainty in assessing hydrological impact of climate change in the Upper Beles River Basin, Ethiopia. *Hydrology Research*, 44, 377–398.
- [38] Yan, R., Gao, J., & Li, L. (2016). Modeling the hydrological effects of climate and land use/cover changes in Chinese lowland polder using an improved WALRUS model. *Hydrology Research*. <https://doi.org/10.2166/hydro.2016.204>